

GAS FLUXING OF ALUMINUM: COMPARISON OF COMPUTATIONAL FLUID DYNAMICS MODELS AND EXPERIMENTS

Autumn Fjeld¹, James W. Evans¹ and D. Corleen Chesonis²

¹Department of Materials Science and Engineering, University of California, Berkeley, CA 94720

²Alcoa Technical Center, Alcoa Center, PA 15069

Keywords: gas fluxing, computation fluid dynamics, two phase mixing, aluminum processing

Abstract

Chlorine fluxing is an essential purification step in aluminum refining in which impurities such as Ca, Na, Li, and Mg are removed by bubbling a mixture of chlorine and argon gas through molten aluminum. The efficiency of impurity removal and control of toxic chlorine and chloride emissions are dependent upon the extent of gas dispersion or mixing, residence time of the bubbles, and surface area of the bubbles. Clearly, these gas phase parameters cannot be directly observed in molten aluminum, thus there are details of the fluxing process which are not fully understood. To gain further insight, two computational models have been developed to simulate the complex two-phase fluid dynamics of a rotary gas injection system. The results of these two modeling approaches are presented and analyzed and compared to experimental bubble measurements gathered using a capacitance probe, which detects bubbles in molten aluminum.

Introduction

With the advancement of computational fluid dynamics packages and ever increasing computational power, mathematical modeling of complex two phase reactor systems has become a viable way to investigate and characterize full scale industrial fluxing operations. Gas fluxing technologies which bubble gas through a stagnant or agitated liquid are commonplace in metallurgical and chemical operations. In the aluminum industry impurities are removed from molten metal in a rotary gas injection vessel, in which chlorine gas is injected from a rotating impeller, providing global mixing in the vessel while facilitating bubble breakup and dispersion of bubbles^{1 2 3 4}. There is a lack of experimental data for important parameters such as bubble size, dispersion and residence time, which determine the productivity of the unit, dictated by the effect of interfacial area on kinetics and by the effect of bubble distribution on mass transfer limitations within the available liquid volume^{1 2 3}. These experimental deficits can be offset by mathematical modeling of the complex fluid dynamics of a rotary gas injection fluxing unit, such as Alcoa's A622. It is the aim of this study to develop a model which incorporates the relevant physics such that the model may be used to improve operations of existing fluxing units and guide future impeller and vessel designs. One might also imagine that such a tool has the potential to be utilized as part of a control strategy in industrial fluxing operations.

Given the complexity of these models and the nature of phenomena such as turbulence which are still not fully understood it is important to establish well defined design objectives and model characteristics which can be tested against meaningful

criteria. Sensible CFD modeling begins with a design objective and modeling scheme complimentary to the flow characteristics or operating parameters of interest. In other words, the time and length scales relevant to the problem will dictate the modeling approach. The Euler-Euler or continuum approach is well suited to model high volume fraction bubbly flows in large scale industrial vessels; the Euler-Lagrangian approach provides a discrete view of the dispersed phase with an increase in computational demand, while volume of fluid or front tracking methods mimic the detailed movement of the interface between two fluids. Model development should also consider the information available which can be used to verify simulation results such that the relevant aspects of the flow or vessel are developed. Common verification sources include experimental flow fields, plant operating data, equipment design specifications, results from similar CFD models and energy check and balances.

Numerous CFD simulations for single phase turbulent flow in agitated vessels can be found in the literature, establishing CFD as a viable tool for investigation of the fluid dynamics in complex systems. Experimental techniques such as particle image velocimetry have provided detailed flow field data for validation and improvement of CFD models^{5 6 7 8 9}. While it is clear CFD is already becoming an important tool for troubleshooting and design of stirred tanks, there remains much room for improvement in this burgeoning field, specifically in the area of turbulence. Resolving the small scale fluid structures will remain computationally prohibitive in practical applications of CFD for some time. Currently, turbulence modeling is implemented to account for effects of turbulence on the bulk flow. The two parameter k- ϵ turbulence model, employing the concept of an isotropic turbulent viscosity, performs surprisingly well for a wide variety of flows. While robust and economic, the assumption of isotropic turbulence is not appropriate for turbulent 3D flows and the model is unable to account for the non-homogenous turbulence throughout the vessel. Thus, in stirred tanks the k- ϵ model gets the job done, but is considered a poor predictor, typically underestimating turbulent kinetic energy and dissipation rate^{6 9 10}. Better predictions of turbulent kinetic energy have been achieved with zonal modeling, adjusting k- ϵ parameters in different zones or by implementation of large eddy simulations and RANS models which significantly increase computational demands^{11 12 13}.

A few publications report CFD simulations of two phase flow in an agitated tank. Lane et al. (1999) modeled a gas sparged tank with a Rushton turbine, including bubble coalescence and breakup models which showed good agreement with experimental data in patterns of gas distribution and trends in local bubble size. Deen

and coworkers compared Sliding Mesh, Eulerian simulations to PIV data and reproduced the presence of gas cavities behind impeller blades observed in experiments⁵. Gentric et al. compare mixing and bubble dispersion in two industrial gas-liquid-solid stirred reactors using a Multiple Reference Frame approach having shown it comparable with Sliding Mesh¹⁰. They report a reasonable agreement of predicted gas hold up with plant data and an underestimation of mixing power.

Despite some of the aforementioned shortcomings, CFD can significantly increase the understanding of the hydrodynamics in complex systems; particularly in very large or hazardous systems or those with nontransparent fluids or toxic materials. Clearly the CFD approach is well suited for the chlorine fluxing of aluminum where high temperatures and a corrosive environment limit experimental investigations. The following report details the Euler-Euler simulations of an industrial fluxing unit and compares the results of these simulations, specifically bubble dispersion, to previous Euler-Lagrangian simulations and experimental investigations.

Modeling Approach

Euler-Euler

The Euler-Euler approach is a rigorous multiphase modeling approach capable of accurately depicting a wide range of flow conditions and phase interactions. FLUENT'sTM Euler-Euler method is based on Ishii's two fluid approach, in which the two phases are treated as a continuum using the concept of phasic volume fractions to represent the relative amount of each phase in a cell of the computational grid¹⁴.

Navier-Stokes Equations. Time averaged mass and momentum equations are solved for each phase and jump conditions are employed at the interfaces between the two phases.

$$\frac{\partial}{\partial t} \rho_i \alpha_i + \nabla \cdot (\rho_i \alpha_i \bar{v}_i) = 0 \quad (1)$$

$$\frac{\partial}{\partial t} \alpha_i \rho_i \bar{v}_i + \nabla \cdot (\alpha_i \rho_i \bar{v}_i \bar{v}_i) + \nabla \cdot (\alpha_i \rho_i \overline{v_i v_i}) = \alpha_i \nabla p + \nabla \cdot \bar{\tau} + \alpha_i \rho_i \bar{g} + F_{int}, \quad (2)$$

where α is the volume fraction of each phase and the subscript i specifies the liquid, $i=1$, or gas, $i=2$, phase. The terms on the left hand side of the momentum equation represent accumulation, convective transport, and turbulent transport of momentum. The terms on the right side represent pressure forces, viscous forces, gravitational forces and interaction forces between the phases.

Interaction Forces. Momentum transfer between the phases is accounted for with appropriate interphase momentum terms describing the gas-liquid interaction in the system. Interphase moment terms include drag as a standard interaction force and may include a number of other interaction forces, depending on the complexity of interactions between the phases. Other interaction terms such as added mass, lift, turbulent dispersion, or Basset forces may be considered relevant if the force is experimentally verified and inclusion of the force in the mathematical model has a significant influence on the simulation¹⁵. In the present model F_{int} takes into account the drag force.

(Turbulent dispersion of the discrete phase is accounted for via the turbulence model.)

$$F_{int} = \frac{18\mu}{\rho_p d_p^2} \frac{C_D Re}{24}. \quad (3)$$

Turbulence. The time averaged Navier-Stokes equations contain additional terms, the Reynolds stresses, which represent the effects of turbulence. The standard k- ϵ turbulence model, which makes use of the eddy viscosity concept, is employed to model these stresses.

$$-\rho \overline{v v} = \mu_t (\nabla v + \nabla v^T) - \frac{2}{3} (\mu_t \nabla \cdot v + \rho k) \delta \quad (4)$$

$$\mu_t = \frac{C_\mu \rho k^2}{\epsilon}, \quad (5)$$

where μ_t is the turbulent viscosity, k is the turbulent kinetic energy, and ϵ is the turbulent dissipation rate.

Model Domain and Boundary Conditions

The geometry of the fluxing box and impeller is shown in Figure 1. The impeller is explicitly modeled. The rectangular geometry adds a unique aspect to our simulations, as most CFD geometries are cylindrical in shape. FLUENT's Multiple Reference Frame (MRF) technique was used to handle the non-axisymmetric rotational motion of the impeller. In this method the domain within the tank is split into a stationary and a rotating sub-domain and the governing equations are defined with reference to each sub-domain's reference frame. The model contained 14,239 cells in the rotating sub-domain and 227,716 computational cells in the stationary sub-domain.

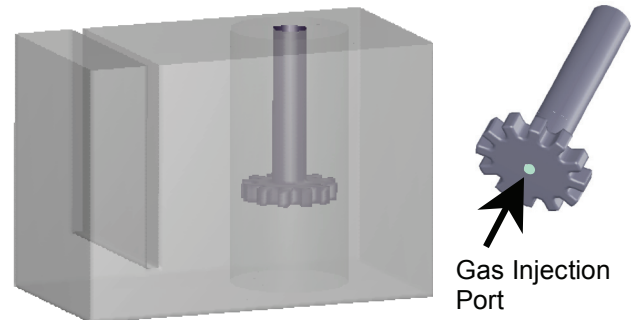


Figure 1. Model geometry: replica of Alcoa's A622 fluxing unit. The impeller is explicitly modeled.

Simulations were carried out as steady state approximations with FLUENT's segregated solver using a co-located scheme where pressure and velocity are stored at cell centers. Pressure-velocity coupling is achieved with the Phase Coupled SIMPLE algorithm. Convergence was achieved when the residuals dropped below 10^{-3} and leveled off to a constant value. Impeller speed was set by specifying a rotational velocity for the rotating sub-domain and specifying the impeller walls as a moving no-slip wall with zero velocity relative to the rotating sub-domain. The tank walls and

bottom were set as no slip. The top surface was specified with a user defined degassing boundary condition, treating the liquid surface as shear free surface while permitting the gas to escape. A surface for the gas inlet was created on the underside of the impeller and set as a velocity inlet.

Euler-Lagrangian Approach

Previous computational models using an Euler-Lagrangian approach were developed with FLUENT's Discrete Phase Model (DPM). Details of the model setup are reported in Fjeld et al. 2005¹⁶ and the model geometry is identical to Figure 1. In the DPM simulation the trajectory of a discrete phase particle, or bubble, is predicted by integrating a force balance equation with reference to the Lagrangian reference frame, as given by

$$\frac{du_p}{dt} = F_D(u - u_p) + \frac{g_x(\rho_p - \rho)}{\rho_p} + F_x \quad (6)$$

where u is the velocity of the fluid, u_p is the velocity of the particle, ρ is the density of the fluid, ρ_p is the density of the particle, and F_x represents additional forces such as pressure gradients, lift, and virtual mass. The drag force is

$$F_D = \frac{18\mu}{\rho_p d_p^2} \frac{C_D Re}{24} \quad (7)$$

where Re is the relative Reynolds number, d_p is the diameter of the particle and C_D is the drag coefficient.

Model Results

Gas Dispersion: Euler-Euler Model

For simplicity in this stage of our Euler-Euler modeling, a single bubble size is specified in each simulation. The effects of bubble size on the gas volume fraction are reported in Table 1. The effect of bubble size on dispersion within the fluxing unit is graphically shown in Figures 2 and 3. The rotor speed was set at 200 rpm with a gas flow rate of 70 L/min (150 scfh) and bubble diameters were specified as 1mm and 10mm in separate simulations. The larger bubbles are driven upwards, with little horizontal drift due to the dominant buoyancy force acting on the bubble. The smaller bubbles in Figure 2 appear more dispersed, experiencing horizontal motion due to momentum transfer from the liquid phase.

	1mm	10mm
Inner Sub-domain	8.93%	4.73%
Outer Sub-domain	2.05%	0.54%
Entire Domain	2.54%	0.84%

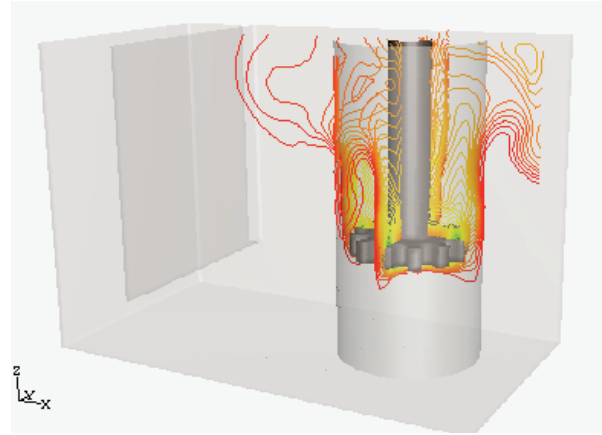


Figure 2. Contours of gas volume fraction in perpendicular planes of the fluxing unit. Impeller speed was 200rpm and gas flow rate 70 L/min (150 scfh) specified as 1mm bubbles.

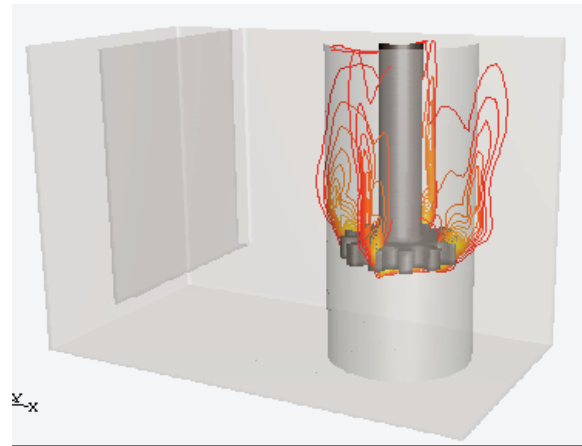


Figure 3. Contours of gas volume fraction in perpendicular planes of the fluxing unit. Impeller speed was 200rpm and gas flow rate 70 L/min (150 scfh) specified as 10mm bubbles.

Bubble Trajectories: Discrete Phase Model

The bubble trajectories predicted in our previous DPM models match the Euler-Euler dispersions fairly well. Bubble trajectories for a simulation which included 1mm, 5mm, and 10 mm bubbles are shown in Figure 4 for the same operating conditions as the Euler-Euler models. The larger bubbles do not travel far from the region surrounding the impeller shaft; however the smaller 1mm bubbles have significant horizontal movement and are dispersed through a greater region of the vessel. The DPM uses injection points to introduce bubbles into the flow field, thus the exact trajectory can be dependent on the chosen injection type and location. However all three bubble sizes were injected from the same location, thus the differences in path trajectory is due to the gas-liquid interactions as a result of different bubble sizes

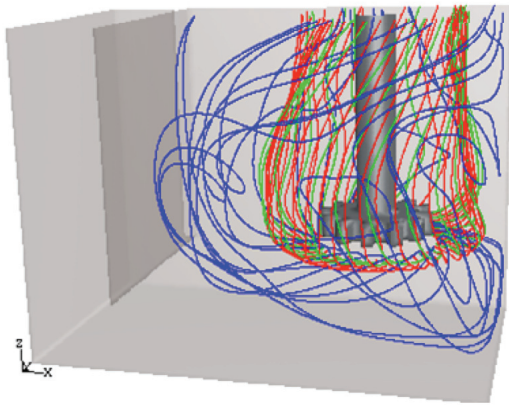


Figure 4. Predicted bubble trajectories from FLUENT's DPM model. Impeller speed was 200rpm with a simulated gas flow rate of 70 L/min (150 scfh). Blue trajectories=1mm bubbles, green=5mm, and red=10mm bubbles.

Model Verification & Analysis

Validation of CFD models can include comparison with experimental data or comparison of general trends with similar modeling investigations. Other common model checks include grid refinement and energy balances. The following analysis of our model results includes comparison with experimental bubble data, comparison with operating data from the plant related to impeller performance, and energy balances. Additionally a number of expressions which predict maximum stable bubble size based on shear or turbulence values are evaluated and compared.

Comparison with Experimental Data

Previous experimental investigations using a capacitance probe, capable of immersion in liquid aluminum for several hours, were carried out to detect bubbles in an industrial fluxing unit at the Alcoa Technical Center¹⁷. The probe was placed at specific locations within each of the zones depicted in Figure 5. The average number of bubbles detected by the probe over a period of two to three minutes is reported as bubble frequency (bub/s). Bubble frequency data has shown the bubbles to be fairly well dispersed in the areas of the fluxing unit, decreasing in observed bubble frequency with increasing distance from the impeller (source of gas injection) as shown in the bar graph of Figure 5. These trends match both the Euler-Euler and the DPM model, which indicate a higher gas fraction or greater number of bubbles near the region around the impeller. Bubbles are still observed in the outer regions of the fluxing unit, however it appears such bubbles are likely to be smaller.

Established operating procedures and published reaction data or impurity removal rates show that sufficient gas liquid contact does occur^{2, 18, 19}. However, what remains as an uncertainty is the exact nature of this contact—bubble size and shape, residence time, distribution throughout the fluxing vessel. From the experimental and model results presented here it appears the gas liquid contact might be thought of as circulating the liquid through a region of high volume fraction near the impeller. Velocity vector fields certainly shown in Figure 6 certainly illustrate this bulk circulation of fluid through the fluxing vessel.

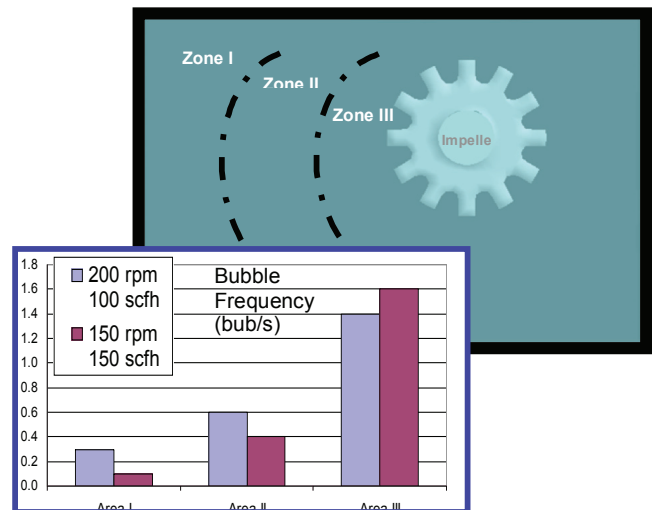


Figure 5. Experimental bubble frequency reported as averages in three zones of the fluxing unit.

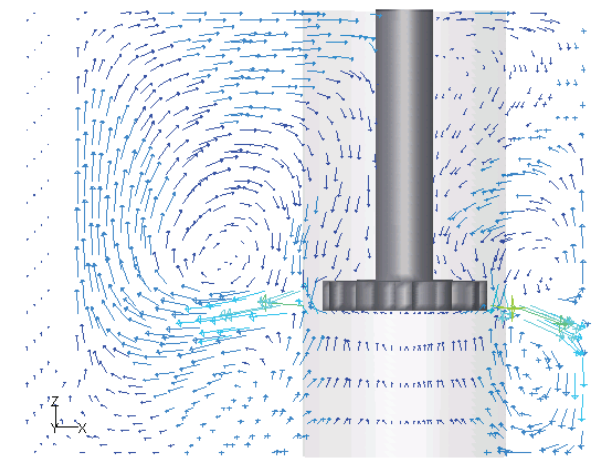


Figure 6. Liquid phase velocity vectors showing the downward pumping of fluid in the near-impeller region.

Impeller Torque and Power Requirements

Impeller specifications or impeller data obtained from the plant can be compared to calculated values of impeller torque and power dissipation from model simulations. The actual power draw reported for this impeller at 200 rpm is 6.5-7.0 amps, 106 V, with a torque of 4.7-6.8 Nm (3.5-5.0 ft-lb). Our model reported values of impeller torque of 5.7 Nm for the 10mm bubble simulation and 11.43 Nm for the 1mm bubble simulation. The match between the plant data and larger bubble simulation and the discrepancy with the smaller bubble is quite interesting and gives weight to the idea that larger bubbles, i.e. those closer in dimension to 10mm than 1mm are found in molten aluminum fluxing units.

Energy Balances.

Comparisons of global energy input and dissipation is possible using the impeller operating data provided by the plant. The total dissipated power can be computed from integration of the turbulent energy dissipation rate over the fluid volume

$$P_{\epsilon} = \rho_{liq} \int \epsilon dV \quad (8)$$

This can be compared with the power input based on impeller torque as reported by the plant and from the calculated torque.

$$P_{Torque} = T_{imp} \cdot \omega \cdot 2\pi \quad (9)$$

where T_{imp} is impeller torque and ω is the rotational speed of the impeller (rpm). Calculated values from these expressions are compared in Table 2. Since values of impeller torque match fairly well with plant operating values of impeller torque, the calculations of impeller power also match well. Prediction of power dissipation in the fluid based on turbulent energy dissipation rates under predicts the maximum plant values by as much as 75%, as is often reported in the literature^{9 6 10}. Additionally, as the bubble size is increased the predicted energy dissipation rate decreases. This is in opposition to impeller torque/power values which increase as bubble size decreases, an effect likely due to the apparent per cell volume fraction at the impeller wall where the torque is calculated. The present simulation employs a mixture k- ϵ model, which uses averaged values of fluid properties based on volume fraction (reported in Table 1). Since this value is taken for the entire fluid volume the simulations which report higher overall gas fraction have significantly different mixture properties, i.e. lower density, lower viscosity. Turbulence models which account for turbulence in each phase may improve predictions of energy dissipation rate and are currently being investigated.

	Plant	1mm	10mm
P_{ϵ}	---	84 W	33.6 W
T_{imp}	4.7-6.8 Nm	11.43 Nm	5.7 Nm
P_{Torque}	98 - 142 W	239 W	119 W

One would expect the model prediction, based on ϵ to be on the low side since the k- ϵ model is known to under predict the energy dissipation rate.

Estimated Bubble Size.

The impurity removal rate in chlorine fluxing is a function of available surface area for reaction, thus a function of bubble size and shape. Due to the lack of experimental bubble data in industrial fluxing units, numerous bubble size correlations have been proposed in the literature^{20 21 22}. Evaluation and comparison of four correlations are presented here. Each is derived from consideration of the balance of forces acting on a bubble: forces which keep a bubble intact (surface tension) versus forces in the surrounding liquid, which promote bubble breakup.

Using an expression from Clift, Grace, and Weber the maximum stable bubble diameter is determined based on a balance, or

imbalance, of surface tension and viscous forces acting on a bubble

$$d_{max} = \frac{\sigma_{liq}}{\tau} - \frac{\mu_{bub}}{\sqrt{\tau\rho_{bub}}} \quad (10)$$

where d_{max} is the maximum bubble diameter, σ_{liq} is liquid surface tension, τ is the shear stress, μ_{bub} is viscosity of the bubble, and ρ_{bub} is density of the bubble²⁰. The maximum reported shear at the impeller was 40 Pa with a corresponding d_{max} of 2 cm.

Rigby and coworkers propose a correlation for predicting the Sauter mean diameter, d_{32} :

$$d_{32} = C_2 \epsilon^{\frac{2}{5}} \left(\frac{We_c \sigma_{liq}}{2\rho_{liq}} \right)^{\frac{3}{5}} \quad (11)$$

where $C_2 = d_{32}/d_{max}$ and We_c is the critical Weber number. Literature values of We_c and C_2 are tabulated for a range of flows in the referred publication²¹.

A related correlation for prediction of the maximum bubbles size in a stirred melt is offered by Johansen and coworkers:

$$d_{max} = \left(\frac{\sigma_{liq}}{\rho_{liq}} \right)^{0.6} \left(\frac{M}{P} \right)^{0.4} \quad (12)$$

where M is the mass of metal in the chamber and P is power supplied to the liquid²². For our 10mm Euler-Euler model M=1217 kg, P~140W. Units for this expression are not reported in the reference and are assumed to be in meters.

Hop et al²³ use a slightly different correlation for maximum bubble size:

$$d_{max} = \sqrt{4} \left(\frac{\sigma_{liq}}{\rho_{liq}} \right) - \frac{1}{\sqrt{\frac{1}{6}g + \epsilon^{\frac{2}{3}} d_{max}^{-\frac{1}{3}}}} \quad (13)$$

The above expressions were calculated using shear values reported at the impeller wall and maximum energy dissipation rates in the region of the impeller. The calculated bubble sizes, which are in good agreement, are summarized in Table 3. The correlation from Hop was evaluated over a range of energy dissipation rates, 25-200 m^2/s^3 , had only a slight effect on d_{max} .53 -.4 cm. The average value is reported below.

Clift	Rigby	Johansen	Hop
2 cm	1.6 cm	2 cm	0.45 cm

Reaction Model

The bubble residence time data have been used in a second model that computes the degree of reaction of the injected bubbles allowing a calculation of the productivity of the fluxing unit and the emission of gaseous chlorides. There is insufficient space to give these results here; they will be presented at the conference and in future publication.

Conclusion

Two mathematical models of the gas fluxing of aluminum have been presented and compared with experimental bubble measurements. The Euler-Euler model, the Euler-Lagrangian model, and our experimental observations have shown similar trends in bubble dispersion through the fluxing unit, with a higher gas fraction near the impeller shaft which tapers off far from the impeller. Variation of bubble size has shown a significant effect on gas holdup, impeller torque, and energy dissipation rate. Analysis of model results indicates that simulations with 10mm bubbles match plant operating data much better than simulations with 1mm bubbles. Although a single bubble size is a significant model simplification, this trend agrees with conclusions in the literature regarding bubble sizes in liquid metals and gas fluxing units.

References

1. Engh A, Sigworth GK. Molten Aluminum Purification. . Light Metals 1982: The Metallurgical Society of AIME, Warrendale, PA, p. 983-1001.; 1982. p 983-1001.
2. Chesonis DC, Yu H. In-Line Fluxing with High Speed Multiple Rotor Dispersers. Light Metals 1997: The Minerals, Metals, and Materials Society, Warrendale, PA.; 1997. p 843.
3. Fu Q, Evans JW. Chlorine Fluxing for Removal of Magnesium from Molten aluminum: Part I. Laboratory-Scale Measurements of Reaction Rates and Bubble Behavior. Metallurgical and Materials Transactions B 1998;29B:971.
4. Fu Q, Evans JW. Chlorine Fluxing for Removal of Magnesium from Molten aluminum: Part II. Mathematical Model. Metallurgical and Materials Transactions B, 29B, p.979. 1998.
5. Deen NG, Solberg T, Hjertager BH. Flow generated by an aerated Rushton impeller: Two-phase PIV experiments and numerical simulations. Canadian Journal of Chemical Engineering 2002;80(4):638-652.
6. Jaworski Z, Dyster KN, Nienow AW. The effect of size, location and pumping direction of pitched blade turbine impellers on flow patterns: LDA measurements and CFD predictions. Chemical Engineering Research & Design 2001;79(A8):887-894.
7. Lane GL, Schwarz MP, Evans GM. Numerical modeling of gas-liquid flow in stirred tanks. Chemical Engineering Science 2005;60:2203.
8. Ranade VV, Perrard M, Le Sauze N, Bertrand J. Trailing vortices of Rushton turbine: PIV measurements and CFD simulations with snapshot approach. Chemical Engineering Research & Design 2001;79(A1):3-12.
9. Ciofalo M, Brucato A, Grisafi F, Torracca N. Turbulent flow in Closed and Free-Surface Unbaffled Tanks Stirred by Radial Impellers. Chemical Engineering Science 51, 14, p.3557. 1996.
10. Gentric C, Mignon D, Bousquet J, Tanguy PA. Comparison of mixing in two industrial gas-liquid reactors using CFD simulations. Chemical Engineering Science 60, p.2253. 2005.
11. Sahu AK, Kumar P, Patwardhan AW, Joshi JB. CFD modelling and mixing in stirred tanks. Chemical Engineering Science 1999;54(13-14):2285-2293.
12. Campolo M, Sbrizzai F, Soldati A. Time-dependent flow structures and Lagrangian mixing in Rushton-impeller baffled-tank reactor. Chemical Engineering Science 58, 1615-1629. 2003.
13. Derksen J, Van den Akker HEA. Large eddy simulations on the flow driven by a Rushton turbine. Aiche Journal 1999;45(2):209-221.
14. Ishii M. Thermo-fluid dynamic theory of two-phase flow. Eyrolles; 1975.
15. Sokolichin A, Eigenberger G, Lapin A. Simulation of Bouyancy Driven Bubbly Flow: Established Simplifications and Open Questions. AIChE Journal 2000;50:1.
16. Fjeld A, Edussuriya SS, Evans JW, A.Mukhopadhyay. Mathematical Modeling Of The Chlorine Fluxing Of Aluminum. Light Metals 2005: The Minerals, Metals, & Materials Society, Warrendale, PA.; 2005.
17. Fjeld A, Evans JW, Chesonis DC. Laboratory and Full Scale Measurements of Bubble Behavior in Gas Fluxing Units. Light Metals 2004, Light Metals 2004: The Minerals, Metals, and Materials Society, Warrendale, PA.; 2004.
18. Sigworth GK. Gas Fluxing of Molten Aluminum, Part 2: Removal of Alkali Metals. Light Metals 2000: The Minerals, Metals, and Materials Society, Warrendale, PA.; 2000.
19. Williams EM, McCarthy RW, Levy SA, Sigworth GK. Removal of Alkali Metals from Aluminum. In: Peterson RD, editor. Light Metals 2000: The Minerals, Metals, and Materials Society, Warrendale, PA, p. 785.; 2000. p 785.
20. Clift R, Grace JR, Weber ME. Bubbles, Drops, and Particles. New York: Academic Press; 1978.
21. Rigby GD, Evans GM, Jameson GJ. Bubble breakup from ventilated cavities in multiphase reactors. Chemical Engineering Science 1997;52(21-22):3677-3684.
22. Johansen ST, Gradahl S, Grontvedt PO, T.Tetlie, R.Gammelsaeter. The Bubble Size and Mass Transfer Mechanisms in Rotor Stirred Reactors,. Light Metals 1997, The Minerals, Metals, and Materials Society, Warrendale, PA, p. 663. 1997.
23. Hop B, Frisvold F, Rasch B, S.T.Johansen. The Fluid Mechanics in the HI10 Hycast reactor. Light Metals 1997: The Minerals, Metals, and Materials Society, Warrendale, PA. p 837.